AD-A100 978 MATHEMATICAL SCIENCES NORTHWEST INC BELLEVUE WASH F/G 20/5
MJOLLNIR ROTATIONAL LINE SCAN DIAGNOSTICS.(U)
MAY 81 E L KLOSTERMAN, P E CASSADY F49620-80-C-0066
UNCLASSIFIED MSNW-1157 AFOSR-TR-81-0533 NL

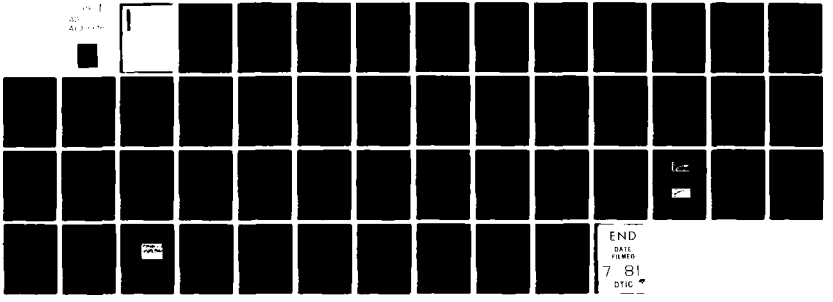

MJOLLNIR ROTATIONAL LINE SCAN DIAGNOSTICS

Final Report

Contract No. F49620-80-C-0066

MSNW-11

E.L. Klosterman and P.E. Cassady

Submitted

19 May 1981

To

AIR FORCE OFFICE OF SCIENTIFIC RESEARCH
Bolling Air Force Base
Washington, DC 20332

By

MATHEMATICAL SCIENCES NORTHWEST, INC.
2755 Northup Way
Bellevue, WA 98004

UNCLASSIFIED

SECURITY CLASSIFICATION OF THIS PAGE (When Data Entered)

REPORT DOCUMENTATION PAGE	READ INSTRUCTIONS BEFORE COMPLETING FORM
1 REPORT NUMBER: AFOSR-TR- 81-0533	2 GOVT ACCESSION NO: AD-A100 978
3 RECIPIENT'S CATALOG NUMBER	
4 TITLE (and Subtitle): Mjollnir Rotational Line Scan Diagnostics	5 TYPE OF REPORT & PERIOD COVERED: Final
6 PERFORMING ORG. REPORT NUMBER: 1157	
7 AUTHOR(s): E.L. Klosterman and P.E. Cassady	8 CONTRACT OR GRANT NUMBER(s): F49620-80-C-0066
9 PERFORMING ORGANIZATION NAME AND ADDRESS: Mathematical Sciences Northwest, Inc. 2755 Northup Way Bellevue, WA 98004	10 PROGRAM ELEMENT, PROJECT, TASK AREA & WORK UNIT NUMBERS: 61102F 2301/A1
11 CONTROLLING OFFICE NAME AND ADDRESS: Air Force Office of Scientific Research Bolling AFB Washington, DC 20332	12 REPORT DATE: 19 May 1981
	13 NUMBER OF PAGES: 43
14 MONITORING AGENCY NAME & ADDRESS (if different from Controlling Office)	15 SECURITY CLASS (of this report): UNCLASSIFIED
	15a DECLASSIFICATION/DOWNGRADING SCHEDULE

16 DISTRIBUTION STATEMENT (of this Report)

Approved for public release; distribution unlimited.

17 DISTRIBUTION STATEMENT (of the abstract entered in Block 20, if different from Report)

18 SUPPLEMENTARY NOTES

19 KEY WORDS (Continue on reverse side if necessary and identify by block number)

Pulsed Laser, Chemical Laser, Diagnostic System.

20 ABSTRACT (Continue on reverse side if necessary and identify by block number)

The rotational line scan diagnsotic technique described in this report can be used to derive the time history of the rotational temperature, the ground state DF population and the population in the first excited state during the output pulse of an atmospheric pressure DF laser from measurements of gain/absorption on three adjacent rotational lines in the 1-0 vibrational band. A description of the theoretical foundations of this technique is given together with sample calculations for typical pulsed DF laser con-

DD FORM 1 JAN 73 1473 EDITION OF 1 NOV 65 IS OBSOLETE

UNCLASSIFIED

SECURITY CLASSIFICATION OF THIS PAGE (When Data Entered)

ditions. An experimental system using a low pressure cw probe laser has been assembled for application on the AFWK Mjollnir laser. The design, assembly, alignment and operation of this diagnostic system are described in detail. Within operational limitations imposed by the probe laser, the performance of the diagnostic system has been verified using a pulsed gain cell.

TABLE OF CONTENTS

LIST OF FIGURES

LIST OF TABLES

I. INTRODUCTION

Among the many parameters that control the performance of pulsed chemical DF lasers, a few specific ones stand out as particularly important. These include the following:

1. Initial gas composition;
2. Initiation power density deposited in the gas as a function of time and spatial location;
3. Initial atom concentration produced by the initiation process;
4. Chemical reaction response of the gas;
5. Temperature rise of the gas as a function of time and spatial location;
6. Optical cavity radiation intensity buildup and laser extraction as a function of wavelength, time and spatial location.

A single diagnostic approach is described in this report that will provide information that is either directly or indirectly related to all of the first five of the important parameters listed above, and will therefore facilitate interpretation of the measurement of the sixth parameter listed above, which is planned as part of the AFWL Mjollnir diagnostic program.

The rotational line scan diagnostic system determines three parameters directly, the DF (v=0) molecular number density, the DF (v=1) molecular number density, and the effective rotational temperature of the DF molecules in the v=0 and v=1 states. These parameters are determined by carrying out time and spatially resolved measurements of the rotational distribution of absorption or optical gain on a number of lines in the 0 - 1 band of DF. This type of measurement was suggested by Avizonis some years ago for use on the CO_2 laser[1] and has been applied very successfully by

MSNW to determine the stored vibrational energy and the gas temperature in the CO_2 gasdynamic laser,[2] in electric discharge CO lasers[3] and in pulsed HF and DF lasers.[4]

By measuring these three parameters, it is possible to determine the following information:

1. The level of pre-reaction of the gas mixture;
2. The spatial nonuniformities in reaction rate, which can be attributed to nonuniform initiation;
3. The initial rate of reaction, which can be attributed to the initial atom concentration produced by the initiation process;
4. The chemical reaction pulse shape as it determines DF in v=0 and v=1;
5. The rotational temperature rise of the gas as a function of time at various locations.

This information will be extremely useful in data interpretation and in comparison with numerical models of the laser.

The theoretical foundations of the rotational line scan diagnostic technique will be described in Section II of this report. The experimental system as tested at MSNW and as applied to the Mjollnir laser is described in Section III. The results of verification experiments carried out at MSNW are also described in Section III. Discussion and conclusions are presented in Section IV.

II. THEORETICAL CONSIDERATIONS

2.1 Rotational Line Scan Measurements of Gain/Absorption on the DF (0-1) Band

Gain and absorption measurements made with a probe laser can be used to calculate the static temperature, the concentration of ground state HF/DF and the ratio of population in the first vibrational level to that in the ground state all as a function of time during the chemical reaction occurring in the pulsed HF/DF chemical laser. This is accomplished by measuring the gain and absorption on several different rotational transitions in the 1 - 0 vibrational band. Under the assumption of rotational equilibrium, the expression for gain/absorption may be written as

$$\alpha_J = \lambda_J^2 \, S \, \frac{A_J}{8\pi} \, \frac{(2J-1)\,\theta\, N_o}{T} \quad \frac{N_1}{N_o} \exp \frac{-\theta J(J-1)}{T} - \exp \frac{-\theta J(J+1)}{T} \qquad (1)$$

where λ_J is the wavelength of the P transition being examined,

S is the lineshape factor equal to $2/Z_c$ in this collisionally broadened case,

Z_c is the collision frequency calculated with optical collision cross sections,

A_J is the Einstein coefficent as a function of rotational level, J is the rotational quantum number of the lower level,

θ is the characteristic rotational temperature,

N_o is the concentration in the ground vibrational state,

N_1 is the concentration in the first vibrational state,

T is the rotational (static) temperature.

Relative gains or absorptions measured in the 1-0 vibrational band are seen to be a function of two unknown parameters: T and N_1/N_o. Plots of relative gain/absorption on several lines in the 1-0 band can be statistically curve fitted to yield values of these two parameters. Once these parameters are so determined, an absolute measurement will yield values for N_o and N_1.

In order to demonstrate the derivation of T, N_1/N_o and N_o from absorption and gain data through the use of Equation 1, several calculations were made with the MSNW pulsed DF laser code described in Appendix A. Conditions were chosen to correspond to the TRW experiments using 8 D_2/21 F_2/71 He initially at 300 ^oK and 1 atm, initiated with a linear growth of F/F_2 to a value of 0.0045 in 4 microseconds.[5] The 89 cm long gain medium was located in a stable oscillator with an output coupling of 60 percent and a loss of 10 percent.

Examination of the calculated output showed that peak output intensity occurred after approximately 3.28 microseconds when the gas temperature was 543 ^oK and the ratio N_1/N_o was 0.48. The absorption and gain for various P transitions in the v=1-0 band was calculated at this time during the pulse as shown in Figure 1. These calculations are based on the assumption of rotational equilibrium. The threshold gain is $5x10^{-3}$/cm in this cavity and only the J=14 line is above threshold and lasing in this band at this time during the pulse.

In order to examine the sensitivity of the gain to T, calculations also were made for 400 ^oK and 300 ^oK. These calculations show that the zero gain intercept and the shape of the positive gain portion of the curve are both very sensitive to changes in temperature in the region of expected experimental conditions. The other parameter

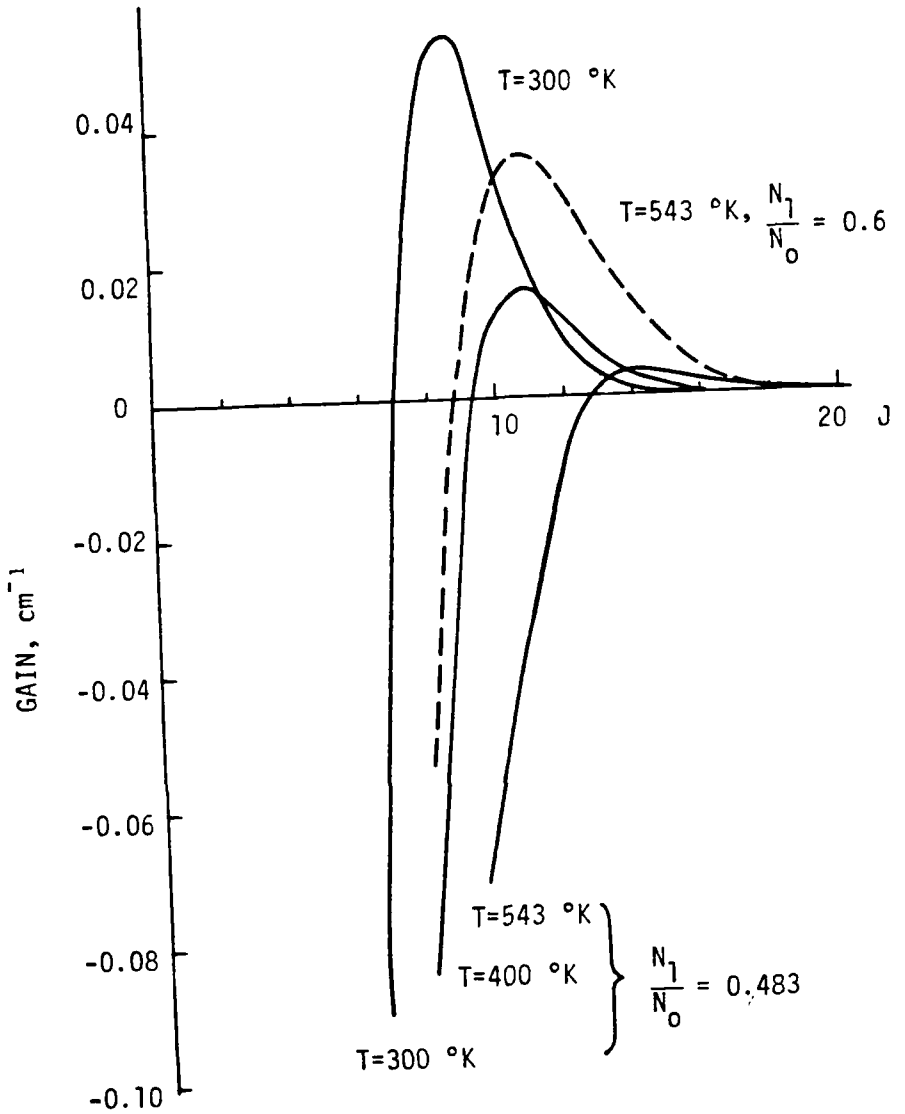

79 03414

Figure 1. Calculated Rotational Gain Distribution v=1-0, 8 D_2/21 F_2/71 He, 300 °K, 1 atm, O.C.=0.60, Loss = 0.10, 89 cm Cavity F/F_2 = 0.0045 in 4 μsec, 3.28 μsec into Pulse.

affecting the gain is the ratio N_1/N_o. Holding T constant at 543 ^oK, N_1/N_o was raised to a value of 0.6 in order to generate a curve having an intercept close to that of the curve for T=400 ^oK, N_1/N_o=0.48. The shape of the resulting curve in the positive gain region is considerably different than that of the 400 ^oK curve.

The calculated amplification factor for the probe laser signal under experimental conditions for a 60 cm pathlength is shown in Figure 2. The MSNW Pulsed DF Laser Code was used to calculate gain values on various V=1-0 lines during the TRW laser output pulse. The amplification and attenuation factors are seen to be of an easily measurable size and the different time histories of the various lines allow meaningful data reduction throughout the pulselength.

These calculations demonstrate that it will not be difficult to derive values for both T and N_1/N_o from the intercept and shape of the distribution of experimentally measured values of gain on several rotational transitions in the v=1-0 band of DF under realistic experimental conditions. The absolute value of the peak gain is related to the absolute number density of ground state DF molecules, so that a value for N_o can be derived from the experimental data as well.

Calculations of the effect of rotational non-equilibrium on gain have been made using the MSNW Pulsed DF Laser code to generate conditions representative of the TRW test case. It was found that rotational nonequilibrium effects reduced the gain by a factor that varied between 20 percent and 38 percent during the output pulselength depending upon the line that was examined. This is a significant reduction, however, it does not affect the feasibility of the measurements.

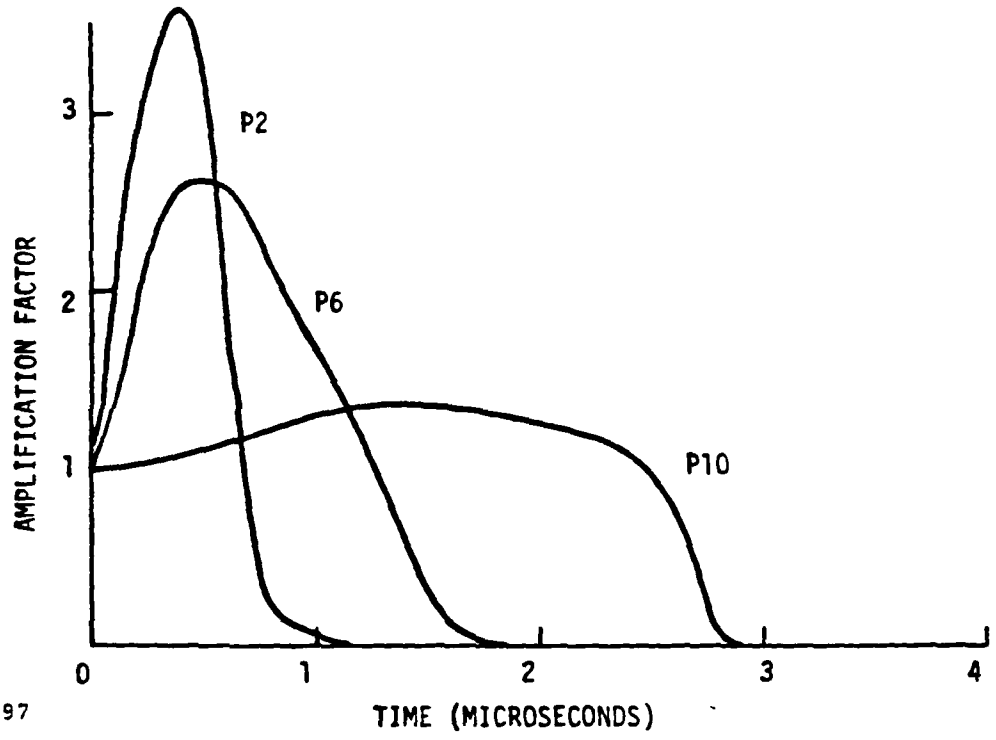

Figure 2. Calculated Amplification Factors During Output Pulse, 8 D_2/21 F_2/71 He, 300 °K, 1 atm, F/F_2=0.0045 in 4 microseconds, 60 cm Probe Pathlength.

7

2.2 Line Broadening and Shift for HF(DF) Lasers

The application of a continuous-wave DF chemical probe laser operating at low pressure (~20 torr) to diagnostic studies of the gain coefficient of a high pressure pulsed DF chemical laser requires the interpretation of the effects of pressure induced line shifts on the measured gain. Because of the low operating pressure of the probe laser, its frequency will be near the vacuum line center frequency, whereas calculations described below show that the Mjollnir laser, operating at 1 amagat, will have it's line center shifted 2 to 3 Doppler widths (half width at half maximum) from the vacuum line center. The gain measured by the low pressure probe laser will differ from the line center value in the Mjollnir laser to a degree that is a function of both the line shift and line width.

A compilation of the data necessary for this correction is presented here for the constituents of the high pressure pulsed DF laser (D_2, F_2, He, SF_6, DF). A considerable amount of data is available for the interaction of HF with itself and foreign gases, while little data is available for DF. Because of the similarities in the intermolecular potentials of HF and DF with the constituent gases, it is expected that the results for DF will be the same as for HF. This assumption is based on the theoretical interpretation that the pressure induced line shift and line broadening are caused by the attractive part of the intermolecular collision processes - primarily induction and dispersion forces.

2.2.1 Line Broadening

Self broadening of DF as calculated by Meredith et al[6] using the resonant-dipole billiard-ball model shows an excellent agreement with the experimental data for HF self broadening. The results of his calculations for DF over the temperature range of 300 ^{o}K to 900 ^{o}K are shown in Figure 3 for the v=1 to v=0 transition.

Effects of foreign gas broadening of HF are shown in Figure 4. Linewidths for broadening by SF_6 and F_2 were obtained from D. F. Smith.[7] The broadening by H_2 and its isotope D_2, obtained from Oskengorn and Vodar[8] is seen to be unusual in that the asymptotic (high J) line width of D_2 is about twice that of H_2. This behavior was confirmed by the data of G. Bacher.[9]

Broadening by He is significantly smaller than the other species, as shown by the one data point obtained by G. Bacher.[10] This value for He is assumed to be essentially constant for all J values, based on the experimental results of D. H. Rank et al[11] for HCl broadened by He.

In addition, the broadening due to Ar, sometimes used as a diluent in pulsed HF(DF) lasers, is shown in Figure 4. The argon data are from the experiments of B. Oksengorn[12] and T. A. Wiggins et al.[13]

2.2.2 Line Shifts

Line shifts in HF by collisions with HF are shown in Figure 5, based on the experimental data of W. F. Herget et al[14] and D. F. Smith.[7] The asymmetry of the line shifts of the P-branch (blue shift) compared to the R-branch (red shift) is also observed in the case of HCl-HCl interactions. A theoretical explanation of this behavior is given by C. Boulet et al[15], who indicate that the first

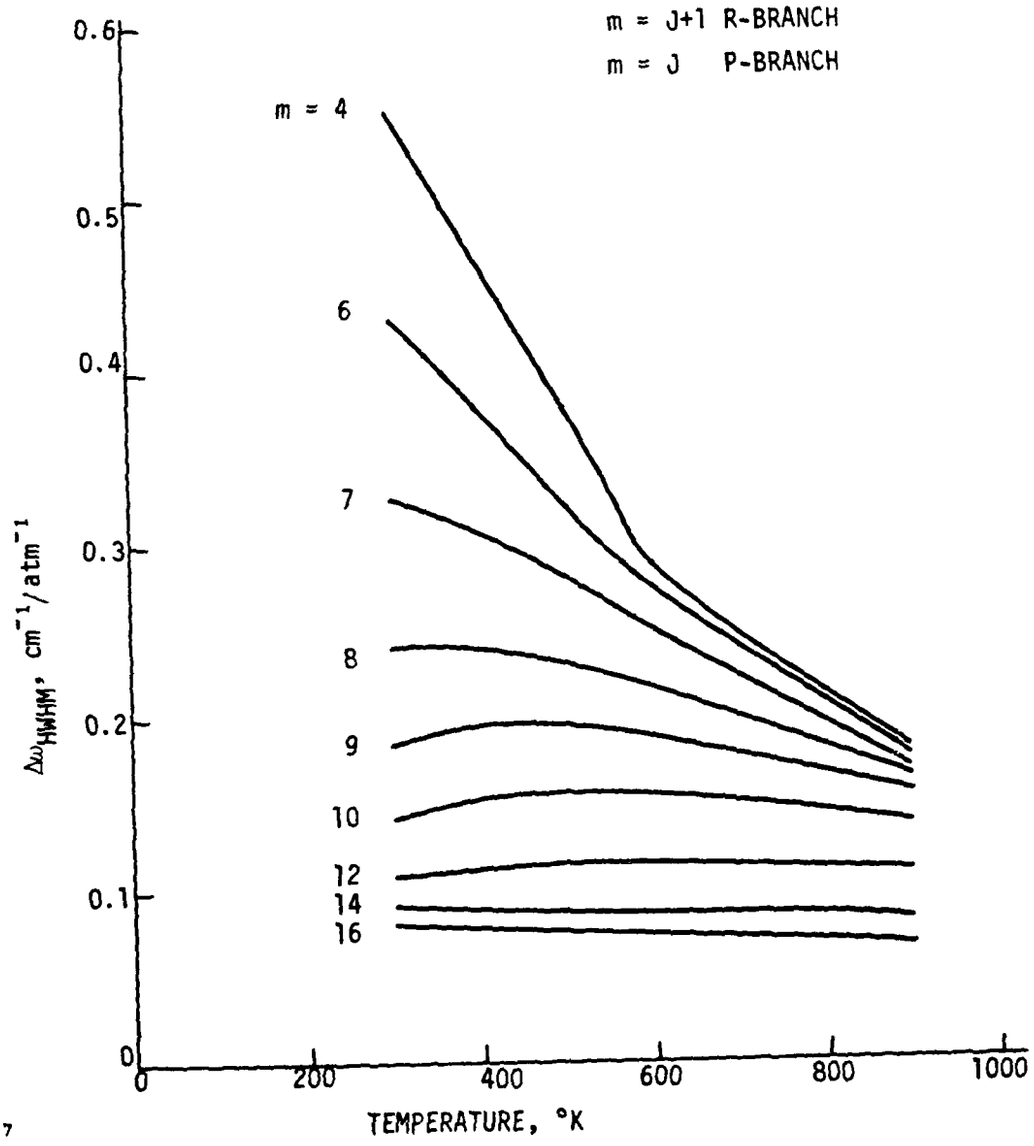

Figure 3. DF - DF Broadening, V = 1-0.

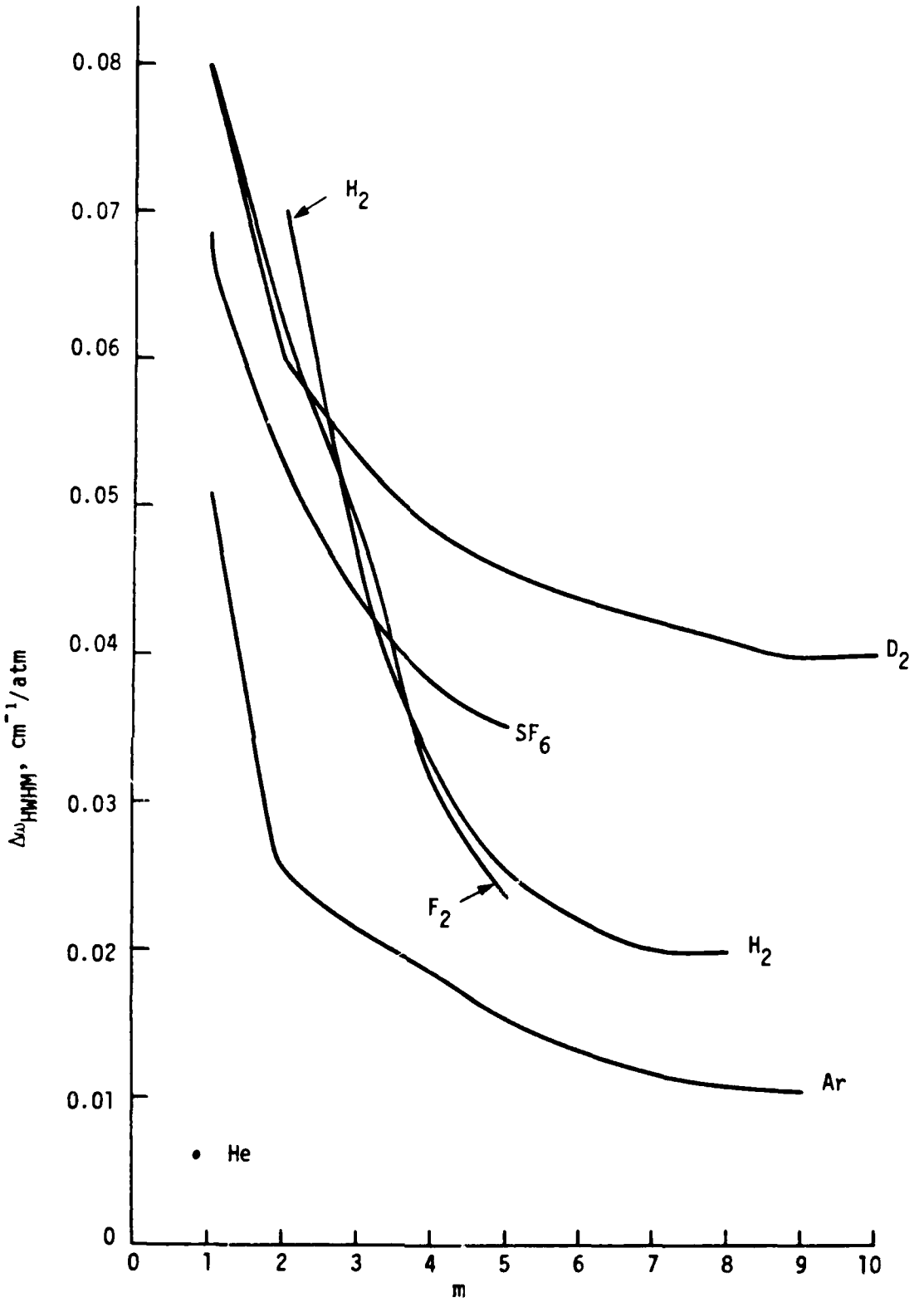

Figure 4. HF Line Broadening by Foreign Gases.

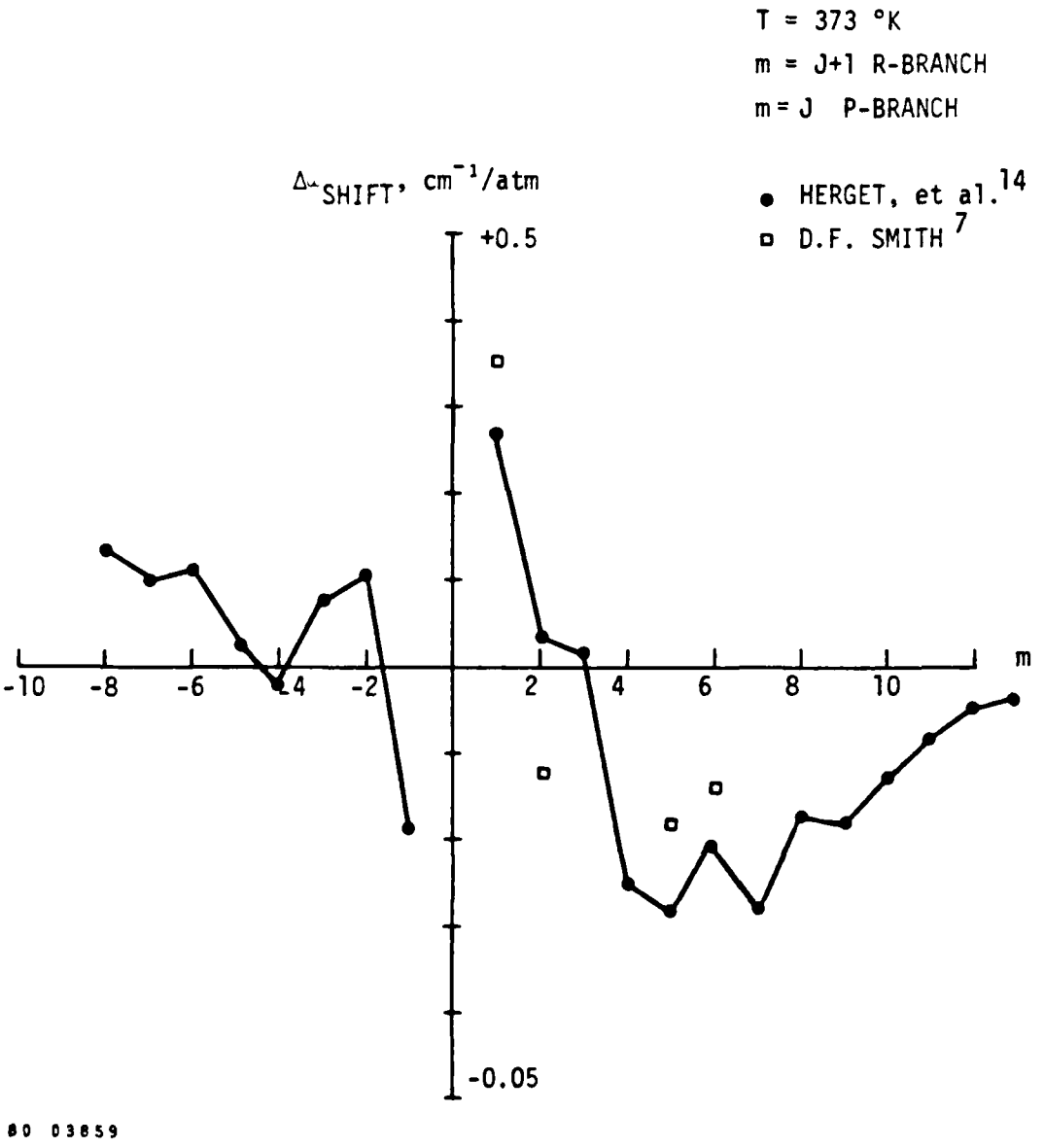

Figure 5. HF - HF Line Shifts.

order contributions to line shift are always negative (red shift), whereas the second order contributions, which are dependent on dipole-dipole interactions, are negative in the R-branch and Positive (blue shift) in the P-branch.

There are little data on the foreign gas line shifting except for noble gases. In general, the foreign gas broadening by non-polar molecules is accompanied by a red shift in both the P- and R-branches. Shown in Figure 6 are the shifts of HF by H_2 and D_2 as measured by Oksengorn and Vodar.[8] It is to be noted that the shifts due to H_2 are comparable in magnitude to the line width ($\Delta\omega$ (HWHM)), whereas for D_2, the shift is about a half of the line width due to D_2.

Since there were no data found for the other pulsed laser gas constituents, a theoretical computation based on the work of J. H. Jaffe et al[16] and A. Ben-Reuven et al[17] was performed. This theory, developed for the interaction of a polar gas with a noble gas (which has spherical symmetry), was fairly successful in computing the shifts for HCl and HF with the noble gases (Ar, Kr, and Xe) but was not applied to He. In addition, the theory predicts only a red shift, whereas in the case of DCl[11] interaction with He resulted in a blue shift. This theory was applied to He and to other molecules to examine its ability to predict the line shift for gases other than noble gases. The results are compared with available experimental data in Table I, for the asymptotic shift at high J values.

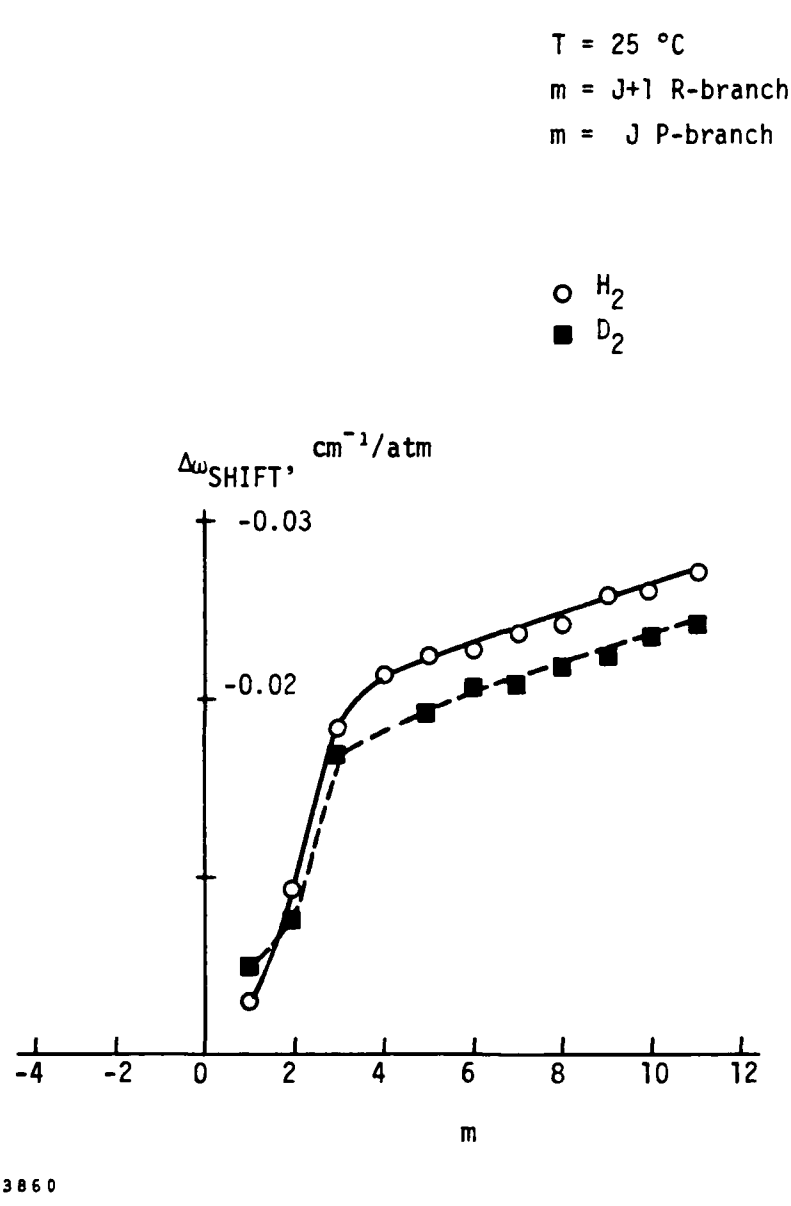

Figure 6. HF - H_2 (D_2) Line Shift.

Table I

Line Shift Computation

	$\Delta\omega$, cm^{-1}/atm Expt	[Ref]	$\Delta\omega$, cm^{-1}/atm (Theory)
He	-		0.003
Ne	0.0025	[18]	0.003
Ar	0.025	[13, 18]	0.028
N_2	0.03	[18]	0.024
SF_6	-		0.042
F_2	-		0.024

Results of the computation for F_2 and SF_6 indicate that the line shifts due to these gases are comparable to the value of line broadening caused by these gases.

The theory predicts a small temperature dependence of the line shift for the gases considered. This has been experimentally verified in the case of Ar at constant density[12]

2.2.3 Impact on Gain Measurements

Broadening and line shift will cause the gain measured by the low pressure probe laser to differ from the line center value in the high pressure laser being examined. In order to estimate the corrections to the gain coefficient measured by a probe operating near the vacuum line center, a plot of the line shape for various pressures as expressed in terms of the parameter a,

$$a = \frac{\Delta\omega_{coll}}{\Delta\omega_D} \sqrt{\ell n 2} \qquad (2)$$

where $\Delta\omega_{col}$ is the collision broadened line width,

$\Delta\omega_D$ is the doppler broadened line width, is presented in Figure 7. For a gas mixture of 20% D_2, 20% F_2, 50% He, 10% SF_6 and at ~1 amagat the value of 'a' will range from ~4.5 to 6.5 during the course of the laser pulse as the reactants are consumed and the temperature rises.

In Figure 8, the ratio of the gain of the laser medium in the Mjollnir laser as measured by the probe relative to that of the Mjollnir media at line center is plotted as a function of the line shift normalized to the Doppler width (HWHM). The plot shows that the gain measured by the probe laser will be between 70 and 90 percent of the line center gain existing in the Mjollnir laser during the output pulse. For the above gas mixture, the line shift will be about 2 to 3 times the laser media Doppler half width. These effects will be time dependent since the Mjollnir laser media will increase in DF concentration and increase in temperature by a factor of 3 to 4 during the laser pulse.

These results show that it will be necessary to perform parallel theoretical calculations in order to interpret gain measurements taken in a high pressure pulsed chemical laser using a low pressure cw probe laser. The MSNW pulsed chemical laser code described in Appendix A is well suited to these calculations. The theoretical analysis described here can be combined with the calculations of this code to provide proper interpretation of gain measurements.

2.3 Probe Laser Mode Spacing

As described above, the gain profile centerline for the high pressure Mjollnir laser is shifted about 1 Doppler full width with respect to the probe laser vacuum centerline frequency. As a result the gain is necessarily being measured off line center in the Mjollnir laser. As seen in

$$a = \frac{\Delta\omega_c \sqrt{\ell n 2}}{\Delta\omega_D}$$

$$\Delta\omega_D = \left(\frac{2kT\ell n 2}{Mc^2}\right)^{1/2} \omega_o, \text{ HWHM}$$

$\Delta\omega_c$ = COLLISION BROADENING, HWHM

ω_o = LINE CENTER

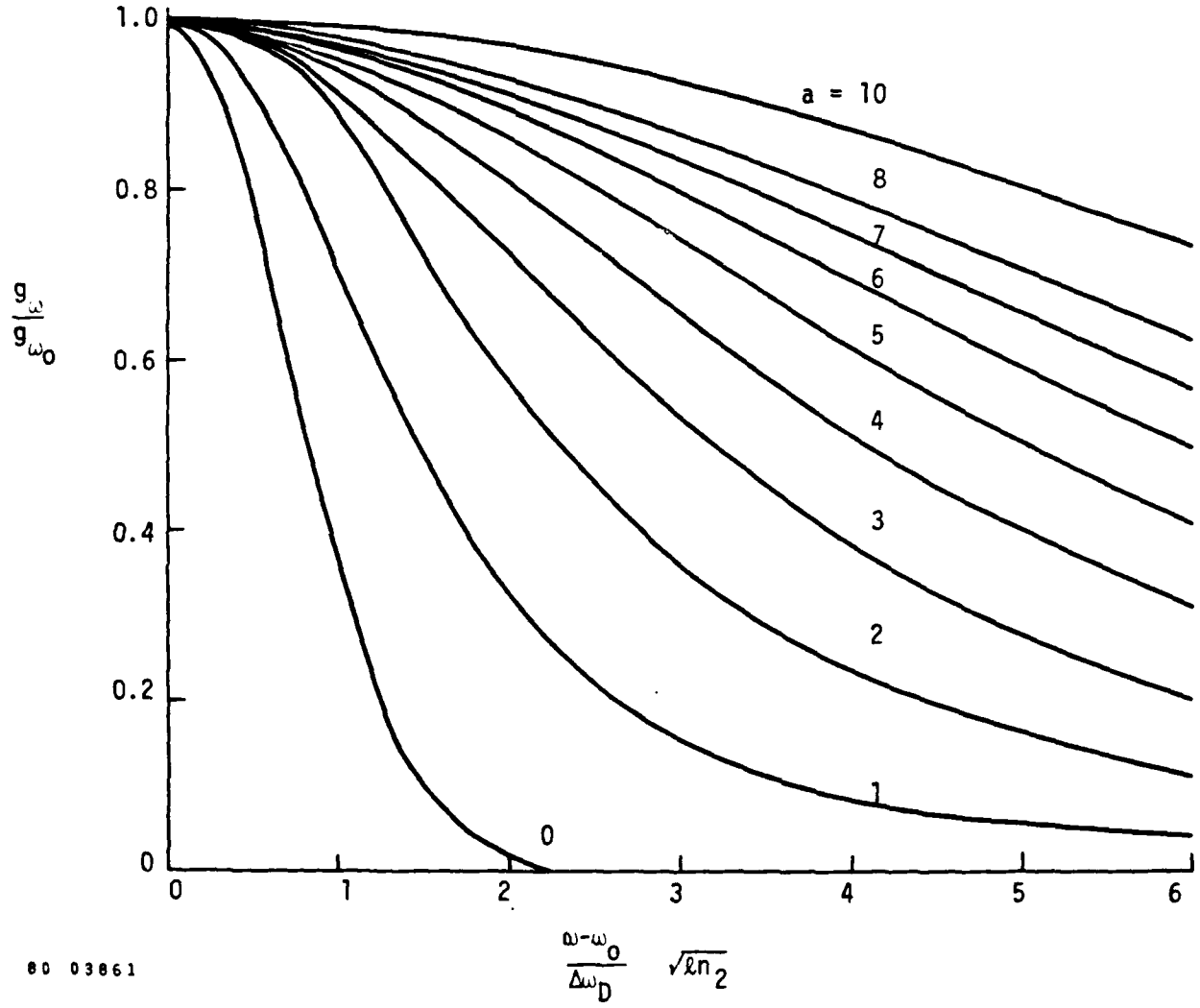

Figure 7. Combined Doppler and Resonance Contour.

$$a = \frac{\Delta\omega_C}{\Delta\omega_D} \sqrt{\ell n 2}$$

$\Delta\omega_D$, $\Delta\omega_C$ ≡ HWHM

$\Delta\omega_{shift} = \omega_{Mjollnir\ line\ center} - \omega_{probe}$

g_{probe} = GAIN MEASURED BY PROBE

$g_{Mjollnir}$ = LINE CENTER GAIN @ MJOLLNIR CAVITY CONDITIONS

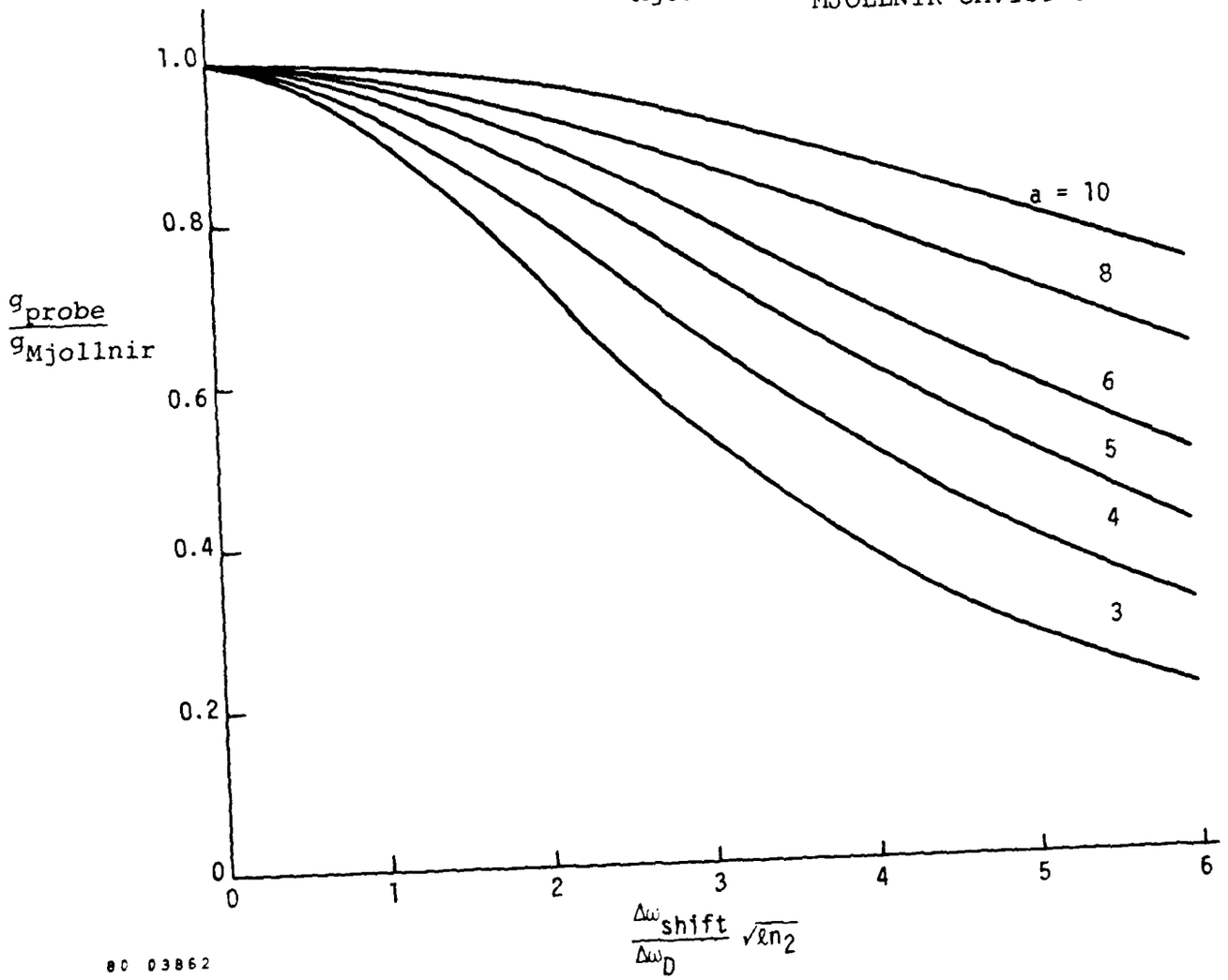

Figure 8. Effect of Line Shift in Laser Cavity on Gain Measurements by Probe at ω_{vacuum}.

Figure 7 the gain coefficient in Mjollnir will exhibit a significant variation with frequency in this region. If the probe laser gain exceeds threshold (and hence lasing possible) over the full Doppler width and if only a single longitudinal cavity mode were to fall within the probe laser Doppler width, accurate measurements of the gain in Mjollnir would be possible only if the frequency of that single longitudinal mode was well known. The 20 to 25 percent gain variation in the Mjollnir laser over a Doppler full width should represent the uncertainty in such a gain measurement.

Since the exact frequency of any single probe laser mode is not known, the probe laser optical cavity can be made sufficiently long that several cavity modes fall within the Doppler profile. The cavity mode spacing is given by $c/2nL$ where c is the speed of light, n is the index of refraction in the medium and L is the physical length between cavity mirrors. For the nominal Aerospace probe laser described in Section III with L = 40 cm, the mode spacing is 375 mHz, greater than the 325 mHz Doppler full width. We have chosen to increase L to a minimum of 185 cm for a mode spacing of 80 mHz. Therefore, there is a cavity mode that is within 40 mHz of the probe laser line center so that based upon Figure 7, the uncertainty in the measured gain in Mjollnir is reduced to about 5 percent.

In this discussion it has been assumed that the probe laser lases only at the cavity mode frequency location that has the highest small signal gain, i.e., at the cavity mode frequency closest to line center. Although the probe laser operating conditions are such that inhomogeneous Doppler broadening is the primary broadening mechanism, the analysis of Mirels[19] suggests that the probe laser operating density is sufficiently high that the active medium maintains a

Maxwellian velocity distribution and therefore avoids hole burning.

III. EXPERIMENTAL SYSTEM

3.1 Design Considerations

The program originally proposed included the use of a Helios cw DF probe laser furnished by the government. Early in the program, AFWL personnel determined that the Aerospace Corporation could more economically supply a low pressure cw multiline HF/DF probe laser capable of operation simultaneously with powers exceeding several 100 mw on several vibrational-rotational lines. Based upon previous Aerospace experience, rotational lines ranging from P(5) to P(14) on the 1-0, 2-1 and 3-2 vibrational bands were expected. This range of vibrational-rotational lines match very well the lasing spectrum in Mjollnir predicted by the MSNW Pulsed DF Laser Code. Furthermore, total output of the laser would be approximately 20 watts. The laser beam diameter was set to be 3 mm and to have a nearly diffraction limited beam divergence of 1.5 mrad.

MSNW conveyed to AFWL and Aerospace the additional requirement that the optical length of the probe laser cavity be considerably longer than the 40 cm planned for the 30 cm active gain length laser. (The details of this requirement are described in Section 2.3). Aerospace, therefore, incorporated into their design a folded cavity giving cavity lengths up to 4 meters.

Based upon the above laser considerations and upon the data requirements for a proper rotational line scan, a system was designed that would allow simultaneous measurement of the gain or absorption on three alternate rotational lines within a single vibrational band, for example, $P_1(7)$ $P_1(9)$ and $P_1(11)$. Imaging lenses were included to control beam size and allow good spatial

resolution of the measurement over long path lengths through Mjollnir (path length > 2 m). The detectors and the data acquisition system were designed with time response on the order of 100 nsec to allow temporal measurement of the gain/absorption on individual lines.

3.2 Details of Gain Measurement System

Figure 9 depicts schematically the laser gain system applied to Mjollnir. The optical components are identified in the figure by numbers with individual specifications called out in Table II. The following short paragraphs describe briefly the key components of the system.

3.2.1 Probe Laser

The laser used as a radiation source for making the gain/absorption measurements is a low pressure, transverse flow, cw chemical reaction HF/DF laser manufactured by Aerospace Corp. The chemical reaction is initiated by F atoms obtained in a low pressure high voltage axial discharge in an $SF_6/He/O_2$ mixture producing about 1 F atom per SF_6 molecule. These discharges occur in a pair of water cooled ceramic tubes approximately 1 meter long. The gas leaves the discharge region at temperatures approaching 700 ^oC and passes through a pair of two dimensional transition sections placed side by side into a 3 mm high by 30 cm wide flow cavity. H_2 or D_2 is injected on the top and bottom walls along the 30 cm width and at a location a few mm upstream of the laser optical cavity centerline. Rapid chemical reaction produces a population inversion enabling lasing. The gas flow is then divided in half before flowing into heat exchangers and finally into a common vaccuum line. Typical laser cavity pressures are 15 to 24 torr. Typical mixtures are $21SF_6/31He/34D_2/14O_2$. Volume flow

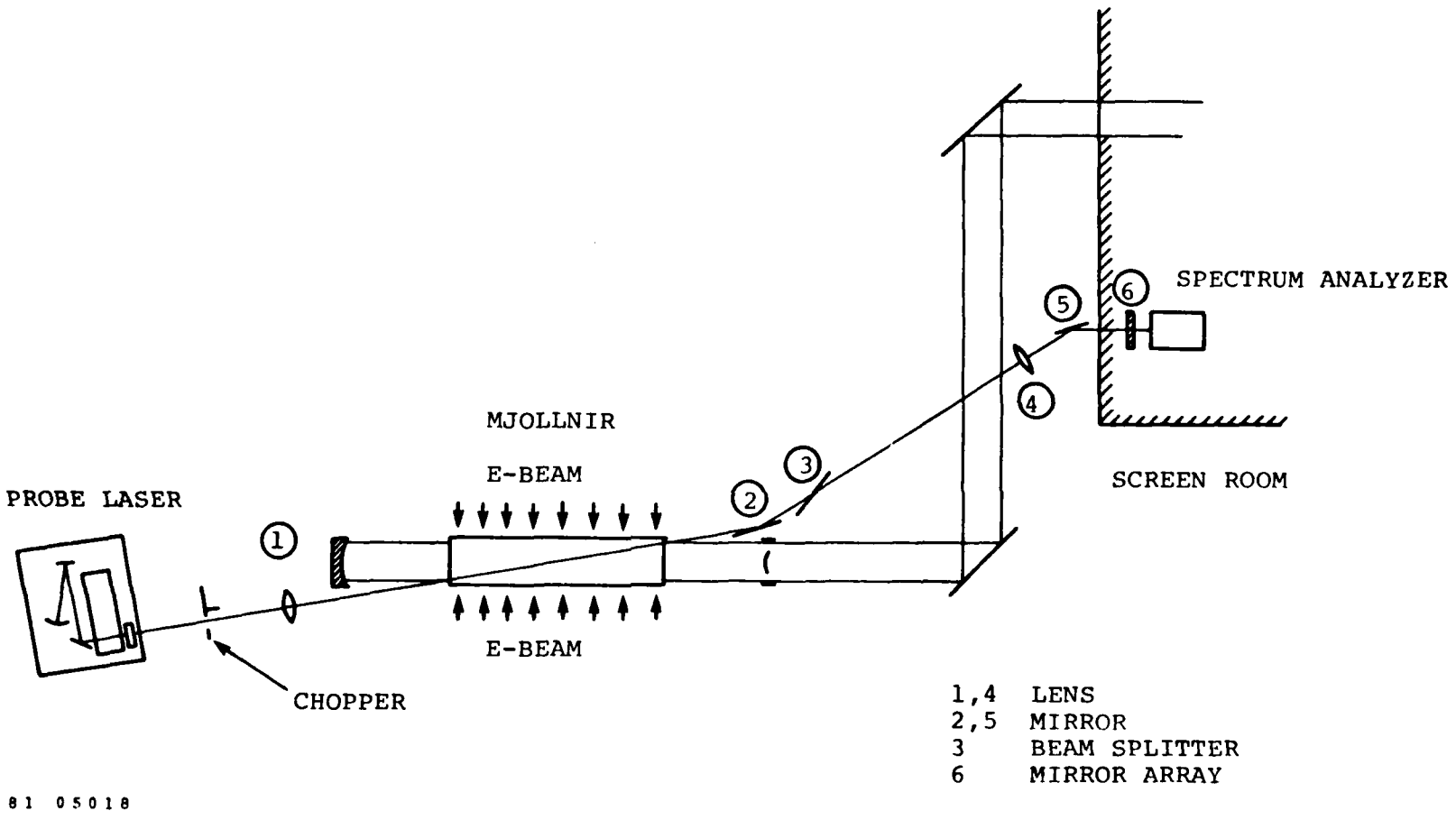

Figure 9. Probe Laser System Arrangement at AFWL.

Table II
Beam Control Optical System Components

No.	Description	Distance From Probe Laser Coupler
1.	CaF_2 lens, 5 cm dia., 150 cm f.l.	300 cm
	Mjollnir Centerline	600 cm
2.	Aluminum coated Pyrex substrate mirror, 5 cm diameter	~800 cm
3.	Uncoated Germanium beam splitter placed at ~45°, 2.5 cm diameter	~850 cm
4.	CaF_2 lens, 5 cm dia., 100 cm f.l.	1100 cm
5.	Aluminum coated Pyrex substrate mirror, 5 cm diameter	~1125 cm
6.	First surface mirror array to direct split beams leave spectrum analyzer to detectors.	1225 cm

rates as high as 450 SCFM are possible with discharge power inputs as high as 17 kV at 0.75 amps.

The laser optical system shown in detail in Figure 10 consists of a flat 10 percent or 20 percent output coupler, several folding mirrors and curved total reflectors. Brewster windows which determine the state of polarization of the laser output are used to couple radiation into and out of the flow cavity. Two curved total reflectors are available, one with a 450 cm and one with a 225 cm radius of curvature. The total optical cavity length suitable with each of the curved reflectors is determined by a Gaussian optics determination so that the TEM_{00} mode size is 67 percent of the 3 mm laser cavity height. For the 225 cm radius of curvature mirror, the optical distance from the curved reflector to the output coupler (which is placed close to the laser cavity) is 185 cm. Specifications for each of the mirrors are called out in Table III.

3.2.2 Beam Control Optics

As shown in Figure 9, several individual mirrors and lenses are used for beam control. The placement of these components with respect to the Mjollnir laser cavity was determined through discussions with AFWL. It was decided that a diagonal path at the shallowest angle possible (determined by the Mjollnir laser mirrors) would be best. The distances of the several elements from the laser output coupler are indicated in Table II.

The probe laser is aimed along the general direction of this path with a mirror available to deflect the beam at the appropriate location. A lens is used to image the probe laser output beam at the center of the path through Mjollnir. Note that a mechanical chopper is used to give a periodic zero reference for the probe beam. Synchronization

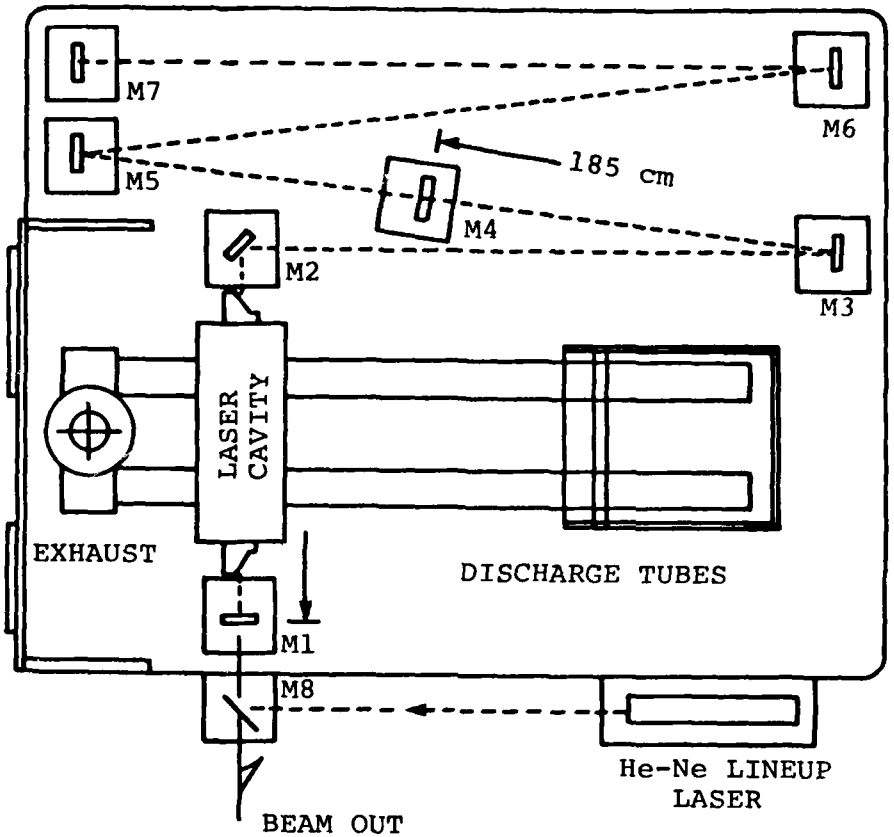

81 05021

Figure 10. Probe Laser Optics Arrangement

Table III
Probe Laser Optical Components

M1	10 or 20% Dielectric Coated Output Coupler, 2.5 cm dia.
M2	Flat Gold Coated Copper Mirror, 2.5 cm diameter
M3	Flat Gold Coated Pyrex Substrate Mirror, 5.0 cm diameter
M4	Gold Coated Metal Mirror, radius of curvature 225 cm, 5.0 cm diameter. Position at 185 cm from output coupler in standard cavity. Removed if using long cavity.
M5,M6	Flat Gold Coated Pyrex Substrate Mirror, 5.0 cm diameter
M7	Gold Coated Metal Mirror, radius of curvature 450 cm, 5.0 cm diameter. Positioned at a distance of 435 cm from output coupler when using long cavity.
M8	Removable Pellicle Beam Splitter for He-Ne Lineup Beam. Removed before HF or DF laser is turned on.

of the chopper with the Mjollnir system is required because of practical limitations on chopper speed. This can be accomplished by monitoring a He-Ne laser beam passing through another slit of the chopper. A second mirror is used to deflect the probe beam in the desired direction towards the screen room. Beyond this, a second lens is used to image and reduce in size the probe beam as it enters the spectrum analyzer in the AFWL screen room. An uncoated piece of germanium can be placed between the second lens and the Mjollnir cavity at a 45 degree angle to help reduce parasitic oscillation between the facing uncoated surfaces of the two lenses. A mirror between the second lens and the screen room is used to properly direct the beam into the screen room. The f number of the beam - second lens combination is chosen to match that of the spectrum analyzer so that virtually all light is collected and displayed. A diffuser may be located at the entrance slit of the spectrum analyzer to eliminate the effect of jitter and refractive disturbances in the Mjollnir cavity. All optical components are mounted on magnetic bases with some permissible adjustment in height. Pedestals and tables as required are to be supplied by AFWL.

3.2.3. Spectrum Analyzer

The spectrum analyzer is an Optical Engineering Model 16-DF which allows the display at the exitplane of resolved vibration-rotational lines in the range of interest. Three separate slits are provided that mount on the analyzer at the proper image point in the exit plane to allow separate measurement of any desired set of three vibrational rotational lines. The slit holders and subsequent splitting mirror assembly are sized to allow simultaneous monitoring of three alternate J lines within a given vibrational band. The mirror assembly has two mirrors at a 45 degree angle to

allow the splitting of the three beams. The radiation which comes through the middle slit passes between the mirrors while that coming out the other two slits is turned through 90 degrees by the appropriate mirror. Once split, the individual beams can be monitored by individual Au-Ge infrared detectors. The data is then acquired and stored in the Biomation data system available at AFWL. For best results, the probe laser polarization should be oriented such that the E-field vector at the analyzer entrance is perpendicular to the grating grooves.

3.2.4. System Alignment

The system is aligned using a He-Ne laser (AFWL suppplied) mounted on a plate attached to the edge of the probe laser base plate. (See Figure 10). A beam splitting pellicle is supplied which mounts in the indicated position. The He-Ne laser is directed by the pellicle to pass through the center of the apertures in the probe laser cavity and then progressively directed by each of the folding mirrors to the total curved reflector which then returns the beam on itself. The reflected beam is then available for aligning the rest of the optical system. However, it is recommended that after alignment of the probe laser cavity the laser output coupler first be placed in the system to reduce the loss in He-Ne intensity within the probe laser optical cavity and to keep the He-Ne beam size as small as possible. Proper alignment of the reflection from the outer surface of the coupler (i.e. surface away from active gain region in the probe laser) is ensured by the parallelism of the two coupler surfaces. The coupler is adjusted so that the reflection of the outer surface is exactly colinear with the path of the reflected beam from the total reflector before placing the output coupler in its path. Once the reflection from the outer surface of the

coupler is available, the alignment of the rest of the optical system is straightforward. The focal lengths of the imaging and reduction lenses are different in the visible than in the infrared so that focal points for the He-Ne will not correspond to those with the infrared beam. Once preliminarily aligned with the He-Ne, the probe laser is turned on and used to verify the alignment. The alignment of the spectrum analyzer can only be verified with the DF probe laser radiation.

3.3 Verification Experiments

The gain measuring system described above for use at AFWL was set up at MSNW for verification testing. All optical path lengths appropriate to the AFWL requirement were simulated. A 10 cm long, fast discharge DF test cell was used to simulate gain or absorption on time scales appropriate to the Mjollnir device. The Aerospace probe laser to be used at AFWL was shipped to MSNW for these tests. An Air Force supplied 35 kw power supply was used to power the laser. A 270 cfm pump available at MSNW was used to evacuate the probe cavity. The paragraphs below describe the experimental results obtained.

The scope of the verification testing program that was possible using the Aerospace probe laser was considerably reduced from that deemed most desirable for complete simulation and verification of the system. In spite of this, the essential features for proper operation of the system have been verified. Sample single line measurements of the gain and absorption in both HF and DF using Au-Ge detectors are shown in Figure 11. The test cell was a blumlein driven fast discharge (lasting 60 nsec) in an 80 to 100 torr mixture of SF_6 and H_2 or D_2. The HF trace at 1 sec/cm shows the rapid rise of gain to 17 percent/cm over

a) HF GAIN/ABS. ON $P^2(7)$

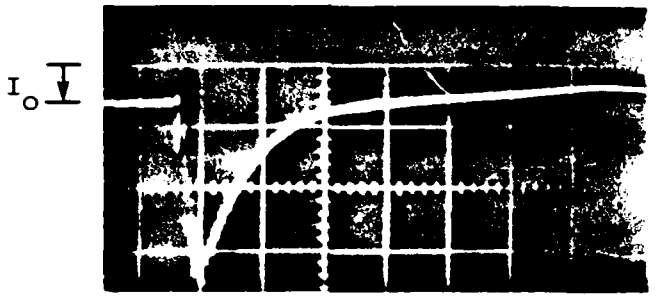

1 μsec/division

b) DF GAIN/ABS. ON $P^2(7)$

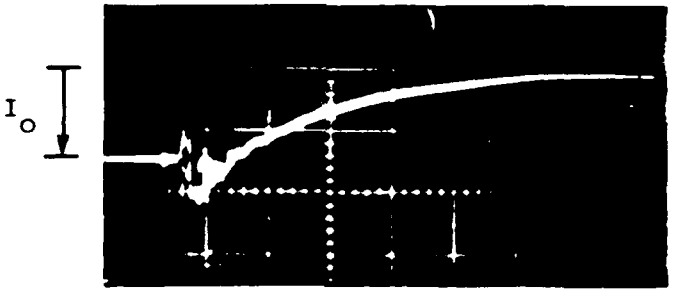

81 05019

1 μsec/division

Figure 11. Oscilloscope Traces if Gain/Absorption Measurements in a Blumlein Driven 10 cm Long Cell for the HF and DF $P^2(7)$ Vibration-Rotation Line.

the 10 cm cell length and then a decay with absorption observed late in the pulse. The magnitude of the gain measured in DF is considerably reduced, about 3.8 percent/cm. The electrical noise at the beginning of each trace had a consistent and reproducible pattern. These traces show that the time response and the signal levels are consistent with diagnostic requirements. No amplifiers were used with the Au-Ge detectors. The traces in Figure 11 are the essential verification data. Due to limitations imposed by probe laser performance it was not possible to simultaneously record three probe laser lines, however three lines were sequentially measured to verify the diagnostic equipment. Two of the three lines have been monitored simultaneously in DF (without the test cell discharge) but were not recorded on photos due to the large variations in power and the limited range in spectral output from alternate rotational lines.

IV. DISCUSSION AND CONCLUSIONS

The limited scope of experimental results was due to many difficulties associated with achieving the expected performance of the laser as outlined in Section 3.1. The shortcomings in laser performance include:

1) considerably reduced range of simultaneous multiline spectral output
2) significant variations in output power on a given vibrational-rotational line on time scales that are short compared to the mechanical chopping frequency but long compared to the 5 to 10 microsecond output pulse length of Mjollnir
3) the large consumption rate of D_2 by the laser and our limited sources of D_2 required considerable operation at HF wavelengths, and
4) build up of residues in the laser flow cavity resulting in considerable reduction and unsteadiness in total laser power.

Of these, 1), 2) and 3) were instrumental in preventing total simulation while 4) required a long effort to achieve adequate laser power for any testing.

The range of spectral output was such that three alternate J lines in a given vibrational band did not lase simultaneously with sufficient power to allow measurement. Furthermore, no lines in the 1-0 band were observed at all. Table IV list the laser transitions observed under widely varying laser operating parameters. These are listed in a manner to convey which lines were seen simultaneously. A brief comment pertaining to the operating conditions (relative to the nominal conditions) of the laser associated

Table IV
Probe Laser Transitions Observed*

DF	$P_2(8)$, $P_2(9)$, $P_3(7)$, $P_3(8)$, $P_3(9)$	18-19 torr full power input
	$P_2(7)$, $P_2(8)$, $P_2(9)$, $P_3(7)$, $P_3(8)$, $P_3(9)$	~13 torr reduced input power
HF	$P_2(9)$, $P_2(10)$, $P_2(11)$, $P_3(9)$, $P_3(10)$	19-20 torr full power input
	$P_2(7)$, $P_2(8)$, $P_2(9)$, $P_3(7)$, $P_3(8)$	15-16 torr reduced power input
	$P_2(7)$, $P_2(8)$, $P_3(6)$, $P_3(7)$, $P_3(8)$	~13 torr reduced power input

* These lines were observed on the more sensitive of the black light lit screens supplied with the optical engineering spectrum analyzer.

with the indicated spectral output is also included. The other feature worth noting from the table is the difficulty in obtaining the lowest J lines in the vibrational bands. This limitation will restrict the information available early in the Mjollnir pulse when low J lines will be above threshold.

The probe laser output power variations on individual rotational lines was very significant even though total output power of the laser was reasonably steady. An example of the type of variation seen for P_2 (7) in HF is shown in Figure 12. Note that the time scale is 2 msec/cm. The fact that the power varies considerably between zero reference chops by the mechanical chopper means that one must be careful about knowing the reference intensity I_o at the time of the Mjollnir lasing. The variations in power with HF could be reduced on a few lines to a few percent by very careful tuning of the probe laser cavity. However, the adjacent rotational lines on either side became so unsteady that they frequently turned off. This, together with other observations, suggested that the power variations might be associated with rotational line competition in which lines closer to threshold suffer more dramatically. This has been verified independently at Aerospace in recent experiments by Bernard.[20] Careful tuning with DF could not reduce the power variations to less than 50 percent over the mechanical chop interval. The strongest DF lines did show power stability over the 5 to 10 μsec time scale needed for the Mjollnir experiment. The essential improvement needed then is to expand the range of simultaneous output, to keep the rotational lines stable enough that none of the lines of interest turn off before or during the Mjollnir experiment and to achieve lasing in the 1-0 vibrational band. The reference intensity level, I_o, at the time of the Mjollnir laser experiment can probably be determined adequately under

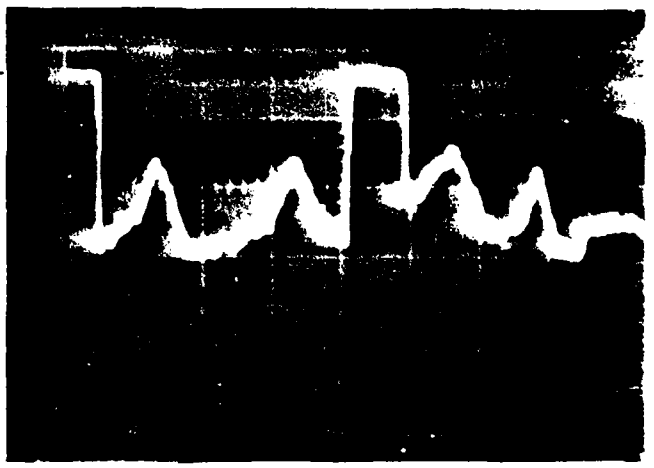

Figure 12. Sample Oscilloscope Trace Showing Temporal Fluctuation of the Laser Power on HF $P_2(7)$.

the present circumstances since the zero level of the detector output remains fixed. It may be necessary to incorporate a reference detector to eliminate uncertainties caused by probe laser output fluctuations.

The origin of the problems associated with residue buildup are unclear. These buildups may be polymerized SF_5 or some other sulfur compounds. The buildup of the residue probably requires periodic cleaning of the laser cavity. Considerable effort was expended in learning that the residues were the instrumental cause in large reductions and oscillations in the total laser output. It is not known what additional impact these residues might have on the stability of the individual lines since the individual lines were monitored only when the total output power was nearly constant.

One final possible contributor to the laser problems is that of an undersized vacuum pump. Aerospace had indicated to MSNW that our 270 cfm pump was adequate. We were, however, unable to run the gas flow rates at the design value and keep the cavity pressure at design levels. This may be a key reason as to why lasing was not observed on the 1-0 band. The gas velocity through the laser region is reduced with reduced pumping capability which may allow the buildup of ground state molecules in the regions of the recessed Brewster windows. The reduced spectral output range could also be a result of limited pumping capacity. We were not, however, able to verify in any conclusive manner the impact of reduced pump capacity.

Within the limitations imposed by the probe laser, the pulsed DF rotational line scan diagnostic has demonstrated the ability to measure gain and absorption on individual rotational lines similar to those expected in the Mjollnir device. Data measured on the Mjollnir device can

be used together with the MSNW pulsed DF laser analytical model to investigate the operating characteristics of the Mjollnir device that are described in Section I.

The particular performance limitations of the probe laser have been documented and described. Several concepts have been developed by MSNW to overcome these performance limitations. These have been described to AFWL technical personnel.

APPENDIX A

MSNW Analytical Model of Pulsed DF Chemical Lasers

MSNW has developed an efficient, realistic analytic model of the pulsed DF chemical laser. This model uses a rapid Gear[21] type numerical integration scheme to follow the time histories of individual vibrational levels. Calculations can be made for rotational equilibrium or rotational non-equilibrium. Intensities are allowed to build up from either background spontaneous emission or from initial levels provided by injection locking. In this manner, the code has been used to model radiative time lag effects. The code monitors the intensities on four neighboring transitions at any given time. This four level manifold is shifted upward as the higher transitions reach threshold and the intensity decays on the lower transitions.

Rotational non-equilibrium has been modeled by the incorporation of a relaxation time which depends on the rotational quantum number, the energy separation between adjacent rotational states and the binary collision frequency with mixture constituents. Incorporation of this rotational relaxation time results in a saturation effect that restricts energy transfer within vibrational levels and produces a lower output intensity with a much more detailed spectral signature.

The kinetic mechanisms include VV deactivation of DF by D_2 and multiquantum VT deactivation of DF by DF and D. The multiquantum deactivation is assumed to be equal probability to any lower vibrational level. The hot and cold reactions are individually followed to determine D and

F concentrations.

This code has been used to model the effects of finite initiation growth rate and radiative time lag on pulsed DF laser performance. This code also has been used to investigate the effects of initiation non-uniformity and intensity non-uniformity in a simplified model of an unstable resonator under the sponsorship of AFWL. The code has proven to be a rapid, inexpensive tool for use in parametric investigations of pulsed DF laser performance. Further description of this analytical model can be found in Reference 22.

REFERENCES

1. P.V. Avizonis, D.R. Dean and R. Grotbeck, "Determination of Vibrational and Translational Temperatures in Gas Dynamic Lasers", App. Phys. Letters, 23, 375-378 (1973).

2. P.E. Cassady, J.F. Newton and P.H. Rose, "A New Mixing GDL", AIAA Journal, 16, 305 (1978).

3. E.L. Klosterman, S.R. Byron and D.C. Quimby, "Supersonic Continuous Wave CO Parametric Investigation", AFWL-TR-76-298 (1976).

4. S.R. Byron, L.Y. Nelson, C.H. Fisher, G.J. Mallaney and A.L. Pindroh, "Molecular Lasers in E-Beam Stabilized Discharges", MSNW Report No. 75-1054, ARPA Order No. 1807 (1975) and L.Y. Nelson, S.R. Byron and A.L. Pindroh, "Electrically Excited D_2 - DF Transfer Laser", MSNW Report No. 75-126-1 (1975).

5. W. Shackleford, C. Merkle, D. Ausherman and R. Aprahamian, "Repetitively Pulsed DF Chemical Laser Program - Final Technical Report" TRW, Redondo Beach, CA (1979).

6. R.E. Meredith, T.S. Chang, F.G. Smith and P.R. Woods, "Investigations in Support of High Energy Laser Technology", Vol I, Science Appl. Inc., SAI-73-004-AA (1973).

7. D.F. Smith, Molecular Properties of Hydrogen Fluoride, 2nd U.N. Geneva Conference, Pergammon Press, 1957.

8. B. Oksengorn and B. Vodar, Compt. Rend., 256, 4870 (1965).

9. G. Bacher, J. Quant. Spectra. Radiat. Transfer, 14, 1280 (1974).

10. G. Bacher, Compt Rend., Series B, 276, 307 (1973).

11. D.H. Rank, D.P. Eastman, B.S. Rao and T.A. Wiggins, J. Mol. Spectry., 10, 34 (1963).

12. B. Oksengorn, Spectrochimica Acta, 19, 541 (1963).

13. T.A. Wiggins, N.C. Griffin, E.M. Arlin, and D.L. Kerstetter, J. Mol. Spectry., 36, 77 (1970).

14. W.F. Herget, W.E. Deeds, N.M. Gailar, R.J. Lovell, and A.H. Nielsen, J. Opt. Soc. Am., 52, 1113 (1962).

15. C. Boulet, D. Robert and L. Galatry, J. Chem. Phys., 65, 5302 (1976).

16. J.H. Jaffe, A. Rosenberg and M.A. Hirshfeld, J. Chem. Phys., 43, 1525, (1965).

17. A.H. Ben-Reuven, H. Friedmann, and J.H. Jaffe, J. Chem. Phys., 38, 3021 (1963).

18. G. Guelachvili and M.A.H. Smith, J. Quant. Spectrosc. Radiat. Transfer, 20, 35 (1978).

19. H. Mirels, "Inhomogeneous Broadening Effects in cw Chemical Lasers", AIAA Journal, 17, 478, (1979).

20. Private Communication.

21. C.W. Gear, Comm. ACM., 14, 176, (1971).

22. P. Cassady, D.C. Quimby and A.L. Pindroh, "Evaluation of Electrical Initiation Methods for Pulsed DF Chemical Lasers", AFWL-TR-79-210, (1979).